Effect of Dissolved Tungsten on the Deformation of 70Ni-30Fe Alloys

K.E. KNIPLING, G. ZEMAN, J.S. MARTE, S.M. KELLY, and S.L. KAMPE

A series of Ni-Fe alloys containing various levels of tungsten in solid solution have been prepared as a means to assess the influence of solid solution strengthening on the mechanical behavior of monolithic 70Ni-30Fe. In particular, 70Ni-30Fe alloys plus equilibrium concentrations of tungsten in solid solution nominally correspond to the compositions associated with the matrix-only portion of certain tungsten heavy alloys, that is, alloys comprised of a high volume fraction of nominally pure tungsten particles embedded within a minority Ni-Fe-W based matrix. The study shows that the working solubility of tungsten within the 70Ni-30Fe base composition increases slightly with temperature, from approximately 21 wt pct at room temperature to approximately 23 wt pct at 1400 °C. Increasing the level of tungsten in solid solution leads to increases in room-temperature yield strength, tensile strength, and ductility. In contrast, the deformation characteristics of the alloys, as quantified by the power-law work-hardening exponent, n, and the strain-rate-sensitivity exponent, m, show little variation with tungsten solute concentration.

I. INTRODUCTION

TUNGSTEN heavy alloys (WHA) represent a unique class of materials developed for applications where their high density can be used to advantage. Alloys that constitute this class of materials include those based on the Ni-Fe-W, Ni-Co-W, or Ni-Cu-W systems, as well as certain alloyed variations of these. These systems enable the production of alloys with high concentrations of nominally-monolithic tungsten while maintaining an ease of processability attributable to the relatively low melting temperature of Ni-rich solid solution phase. Specifically, the alloys are typically processed and densified by means of a powder-based liquid-phase sintering methodology where the solid tungsten particles are embedded within a low-melting Ni-based matrix. Indeed, the two-phase microstructure that results enables one to view this material as an *in-situ* derived metal-metal composite, with a distinctive ductile matrix and isolated, higher-strength tungsten reinforcement.

Considerable alloy development has established compositional and processing influences on the mechanical behavior of tungsten heavy alloys.[1–10] With regard to the Ni-Fe-W system, alloys with Ni:Fe composition ratios of approximately 7:3 (by weight) have emerged as baseline alloys for study, presumably due to this composition's proximity to a freezing point minimum, and as a composition where the formation of certain cooling-rate-sensitive, undesirable intermetallic phases, which adversely affect mechanical behavior, can be avoided.[3,4] While other studies have suggested that other compositions may offer a superior combination of properties, they nonetheless make their comparisons to the properties that have been established for the 7:3 composition.[5–10]

It is generally accepted that the ductility, toughness, and impact resistance values that are measured for the tungsten heavy alloys rely in great part on the physical metallurgy of the matrix phase, that is, on the microstructural details of the continuous Ni-Fe-W solid solution that envelopes the tungsten particles. However, most of our current understanding in this regard has been gleaned from data obtained from full composite samples, *i.e.*, from alloys that typically contain tungsten concentrations of 80 pct or more.[1–10] For example, Ekbom *et al.*[6,7] have shown that strain partitioning to the Ni-Fe matrix occurs early in the deformation of these alloys, leading them to infer that the ductile matrix experiences increased rates of work hardening. Coates and Ramesh[8] likewise measured the hardness of individual phases within a composite Ni-Fe alloy containing 90 wt pct W following high-strain-rate deformation, and have inferred that the matrix phase likely exhibits a higher strain-rate sensitivity that the tungsten phase in these alloys. Rabin *et al.*[1,2] have been successful in associating many of the mechanical dependencies observed in high tungsten alloys to the details of the tungsten (particle)-matrix interface (many of which are established by processing), but only discuss the importance of the inherent flow behavior of the matrix in a relative, general way. Gero *et al.*[10] have studied the fracture of a series of tungsten particle containing variants, and delineate the role of a relatively deformable matrix in the events leading to, and comprising, fracture. In each of these examples, characteristics of the ductile matrix phase have been inferred from the behavior of the full composite composition(s).

There have been relatively few studies that have examined the mechanical behavior of the matrix phase in the absence of the tungsten particle; only the published works of Ekbom *et al.*[6,7] and Woodward *et al.*[11] have provided any tensile or compressive stress-strain data for Ni-Fe-W matrix compositions without the W particles present in full composite formulations. Thus, a comprehensive study that evaluates the mechanical behavior of the matrix phase in isolation of the tungsten particles will provide a clearer and unobstructed

K.E. KNIPLING, Graduate Research Assistant, is with the Materials Science and Engineering Department, Northwestern University, Evanston, IL 60208. G. ZEMAN, Senior Metallurgical Engineer, is with Advanced Technology, Aerojet Ordnance Tennessee, Jonesborough, TN 37659. J.S. MARTE, Materials Scientist, is with the Ceramics and Metallurgy Technologies Group, GE Global Research Center, Schenectady, NY 12301. S.M. KELLY, Graduate Research Assistant, and S.L. KAMPE, Associate Professor, are with the Materials Science and Engineering Department, Virginia Tech, Blacksburg, VA 24061-0237. Contact e-mail: kampe@vt.edu

Manuscript submitted September 9, 2003.

understanding of how the matrix component responds to composition, heat treatment, and testing methodology. Indeed, such information is fundamental for conventional micromechanical modeling of multiphase alloy (composite) behavior.

This study will primarily examine the role of tungsten concentration within the Ni-Fe matrix based on the 7:3 Ni:Fe composition. When incorporated as a component of an *in-situ* processed composite (*i.e.*, a matrix plus monolithic tungsten particles), the Ni-Fe solid solution will additionally contain a thermodynamically dictated concentration of W. Presumably, the presence of tungsten in the solid solution will influence the strength and deformation characteristics of the matrix alloy.

A series of experiments were conducted to establish if solutionization temperature affected W concentration within the matrix phase, and how this would ultimately affect its mechanical performance. Specifically, the solubility of tungsten in the 7:3 Ni-Fe base composition has been determined over a range of submelting temperatures from 800 °C to 1400 °C. Based on this information, ingots were produced by casting with W concentrations corresponding to 0, 30, 70, and 100 pct of the determined solubility limit. These samples, plus non-heat-treated (as-cast) variants, were subsequently evaluated in uniaxial tension to provide yield stress, tensile strength, ductility, work-hardening, and strain-rate-sensitivity information.

II. EXPERIMENTAL PROCEDURE

A. *Solubility Determination*

A series of ingots were produced for the purpose of determining the solubility of tungsten in a solid solution of Ni-Fe. Elemental powders of Ni, Fe, and W were blended in a formulation corresponding to a nominal composition of 49Ni-21Fe-30W; this composition was selected to maintain a Ni-to-Fe wt pct ratio of 7:3. The blended powder was uniaxially cold pressed into several 12.7-mm diameter and approximately 10-mm high cylindrical compacts.

For each of the three ingots that were ultimately produced, approximately six compacts were placed along the length of a 50 mL alumina crucible. The assembled compacts were placed within the hot zone of a resistance-heated vacuum furnace and heated to 1500 °C and held for 1 hour to effect melting of the ingot. During the course of melting, pressure was maintained to approximate levels of 1.3×10^{-7} atm (10^{-4} torr) or less. Following the 1-hour soak at temperature, the ingot was cooled at an average rate of approximately 30 °C/min. To ensure effective homogenization, the ingot was overturned in the crucible and the melting procedure repeated. The resulting ingots were roughly ellipsoidal in cross section, approximately 9.5 mm in diameter, with lengths of approximately 64 mm.

The as-solidified ingots were subsequently sectioned to create eight samples, each approximately 8-mm long, to be used for solubility determination. The samples were wrapped in titanium foil and hermetically sealed under dynamic vacuum within quartz ampules. Heat treatment was conducted by placing the sealed ampules within the temperature-stabilized hot zone of a laboratory tube furnace. Samples were heat treated at 800 °C, 1000 °C, 1200 °C, and 1400 °C for 24 hours, followed by a rapid ice-water quench (imposed by breaking the ampule while submerged).

Following heat treatment, the samples were embedded in 25-mm epoxy metallographic mounts, and polished using standard metallographic techniques. Fresh-polished samples were subsequently microstructurally examined using back-scattered scanning electron microscopy (BSEM), and quantitatively evaluated using spectrographic (energy dispersive) electron microprobe analysis (EMPA). Both analyses (*i.e.*, BSEM and EMPA) were simultaneously conducted using a Cameca model SX50 electron microprobe (Paris, France), thereby enabling phase-specific spectrographic analysis of the two-phase (Fe-Ni-W solid solution and W-rich precipitates) structure. The resolution (spot size) of the microprobe is approximately 1 μm.

The solubility analysis performed on the first set of alloys was confirmed by the production of a fourth ingot, with a nominal composition of 52.5Ni-22.5Fe-25W. This composition maintains the 7:3 Ni:Fe ratio, and was selected on the basis of the analytical results of the first series of alloys as a composition closer to the determined solubility limit of W in the Ni-Fe over the range of heat treatment temperatures examined. This ingot was given a 1200 °C/24-h heat treatment under identical conditions as those described previously.

B. *Alloy Preparation*

Once the temperature dependence of solubility was established, ingots were produced with W compositions corresponding to 0, 30, 70, and 100 pct of the determined full-solubility level (as determined from the experiments described previously), while maintaining the 7:3 ratio of Ni:Fe. The ingots were ultimately subjected to solutionization heat treatments at 800 °C and 1200 °C. As will be shown in Section III, tungsten solubility in the 7:3 Ni:Fe phase exhibited very little variation with temperature between 800 °C and 1400 °C. Ingot precursors were formulated from blended Ni, Fe, and W elemental powders and were cold isostatically pressed into 51-mm-diameter cylindrical compacts. Approximately 125-mm-high sections of the compacts were placed within 55-mm i.d. × 100-mm-high alumina flat-bottom crucibles for melt processing. Ingots were produced by vacuum melting at 1500 °C for 1 hour and were followed by an approximate 10 °C/min (controller controlled) cooldown to room temperature. This processing sequence resulted in an ingot of approximately 1.3 kg in mass, 54 mm in diameter, and 62 to 76 mm in height.

Sections of each produced ingot were submitted to Luvak, Inc. (Boylston, MA), for chemical analyses of major elements (*e.g.*, Ni, Fe, and W) *via* direct current arc emission spectroscopy, and to Colorado Metallurgical Services (Denver, Co), for analyses of interstitials (C, N, and O) by combustion infrared detection.

The density of the ingots was measured using Archimedes method, *i.e.*, by comparing the mass of the sample in air *vs* that measured in water. Samples, approximately 5 g in mass, were obtained from machined sections of the ingot. Approximately ten independent measurements were obtained for each ingot composition produced.

C. *Mechanical Characterization*

1. *Sample preparation*

Tensile blanks were machined from as-solidified ingots using wire electrodischarge machining. In this regard, full-length, 7.5-mm-diameter blanks were removed from random

locations within the cross section of the ingot. Prior to finish machining, titanium-foil wrapped blanks were subjected to heat treatment within vacuum-encapsulated quartz ampules at 1200 °C for 2 hours, then furnace cooled (FC) at a rate of approximately 25 °C/h. Following heat treatment, the tensile blanks were final machined into subsized, button-head tensile specimens with a gage diameter of 3.175 mm and a gage length of 28.575 mm.

2. *Tensile testing*

Three variations of a standard uniaxial tensile test were conducted in an attempt to maximize and survey the nature of the mechanical response of these alloys.

a. *Constant extension-rate testing*

A standard, constant extension-rate test was conducted, utilizing an initial strain rate of 2×10^{-4} s^{-1}. This test provided conventional yield stress (0.2 pct offset), tensile strength, and ductility (plastic strain at fracture) for each sample. In addition, work hardening was quantified through calculation of the work-hardening coefficient, n, obtained from a fit of the experimental data to the Ludwik form of a power-law flow stress equation:[12]

$$\sigma = \sigma_o + K_1 \cdot \varepsilon_p^n \quad [1]$$

where σ is the true flow stress, σ_o is a reference stress approximately equal to the proportional limit, ε_p is true plastic strain, and K_1 and n are microstructure-dependent material constants. The reported results represent an average from two independently conducted tensile tests.

b. *Strain-rate change tests*

Selected variants were subjected to uniaxial tensile tests that additionally included a series of strain-rate changes, or "jumps." In these instances, the tests were initiated using a strain rate of 1×10^{-4} s^{-1}. At an approximate strain value of 5 pct, the strain rate was instantaneously increased to 2×10^{-4} s^{-1}, at 7.5 pct, it was increased to 5×10^{-4} s^{-1}, and at 10 pct, it was increased to 1×10^{-3} s^{-1}. At 12.5 pct strain, the strain rate was sequentially stepped down in reverse order in 2.5 pct strain increments. This procedure enables one to quantify the strain-rate sensitivity of the material, to determine yield stress and tensile strength as a function of strain rate, and to assess whether the strain-rate dependence relies on the accumulated strain within the sample.

Strain-rate sensitivity was quantified by determining the value of the strain-rate exponent, m, for a fit of the experimental data to an equation of the form

$$\sigma = K_2 \cdot \dot{\varepsilon}^m \quad [2]$$

where σ is the measured true flow stress, $\dot{\varepsilon}$ is the true strain rate, and K_2 and m are microstructure-sensitive material constants. The reported strain-rate-sensitivity values represent the average of seven jumps imposed during the course of a single tensile test.

c. *Strain aging tests*

Two selected variants were subjected to tests to evaluate strain aging effects in these alloys, that is, strengthening attributable to static aging following deformation. In this instance, a constant extension-rate tensile test (initial strain rate of 2×10^{-4} s^{-1}) was terminated at approximately 10 pct strain. The load on the sample was mechanically removed, and the sample remained in the testing fixtures under zero load for approximately 65 hours. The test was then resumed using the same extension rate, and the flow stress increase (relative to its value prior to unloading) was recorded. At approximately 15 pct strain, the load was again mechanically removed and the sample allowed to age for 24 hours at which time the loading was reapplied and the test was allowed to proceed until sample failure occurred.

3. *Hardness measurements*

Vickers hardness was measured from the surface of machined tensile samples, using a 50-kg$_f$ load. The measurements were taken from a location on the outer radius of the grip section; cylindrical surface corrections were applied in accordance with the procedure outlined in ASTM E92.[13]

III. RESULTS

A. *Solubility Determination*

Figure 1 illustrates a typical microstructure resulting from a solutionized and ice-water quenched 52.5Ni-22.5Fe-25W sample, utilizing BSEM. These micrographs indicate the presence of tungsten-rich precipitates (light phase) within a crystalline (as verified by X-ray diffraction) Ni-Fe-W single-phase matrix (darker). The matrix grain size, as delineated by a necklace precipitate structure, appears to be approximately 300 μm. The microstructure is nominally similar for all solutionization temperatures employed. The microstructure suggests that the alloy composition is such that the solubility of tungsten in the Ni-Fe matrix has been slightly exceeded. Similar microstructures were observed in the works of Ekbom[7] and Woodward *et al*.[11] for reported nominal tungsten compositions of 23 and 23.4 wt pct respectively.

Table I summarizes the results from the EMPA compositional analyses. In each instance, the probe was programmed to traverse a section of the microstructure along a 100-μm length, analyzing in 1-μm increments. The results given in Table I represent an average of several analyzed points from several analyzed lengths.

Figure 2 depicts the data from Table I, showing the temperature dependence of tungsten solubility within the Ni-Fe-W solid solution (matrix). This figure suggests that the solubility limit of W in 70Ni-30Fe is relatively independent of temperature between 1000 °C and 1400 °C, increasing only slightly between room temperature (≈21 wt pct) and 1400 °C (≈23 wt pct), generally consistent with similarly obtained results in References 7, 11, and 14.

B. *Alloy Production*

Given the results of the solubility study, ingots were formulated with W concentrations of 0, 7, 16, and 23 wt pct, corresponding to 0, 30, 70, and 100 pct of the determined full solubility limit of W in the 7:3 Ni-Fe base composition. As mentioned in Section A and shown in Figure 2, the solubility limit of W for all temperatures between 800 °C and 1400 °C was determined to be approximately 23 wt pct; thus, formulations were essentially independent of solutionization temperature. Table II gives the formulated and actual analyzed compositions for the four ingots produced. Table III provides measured densities as compared to a rule-of-mixtures

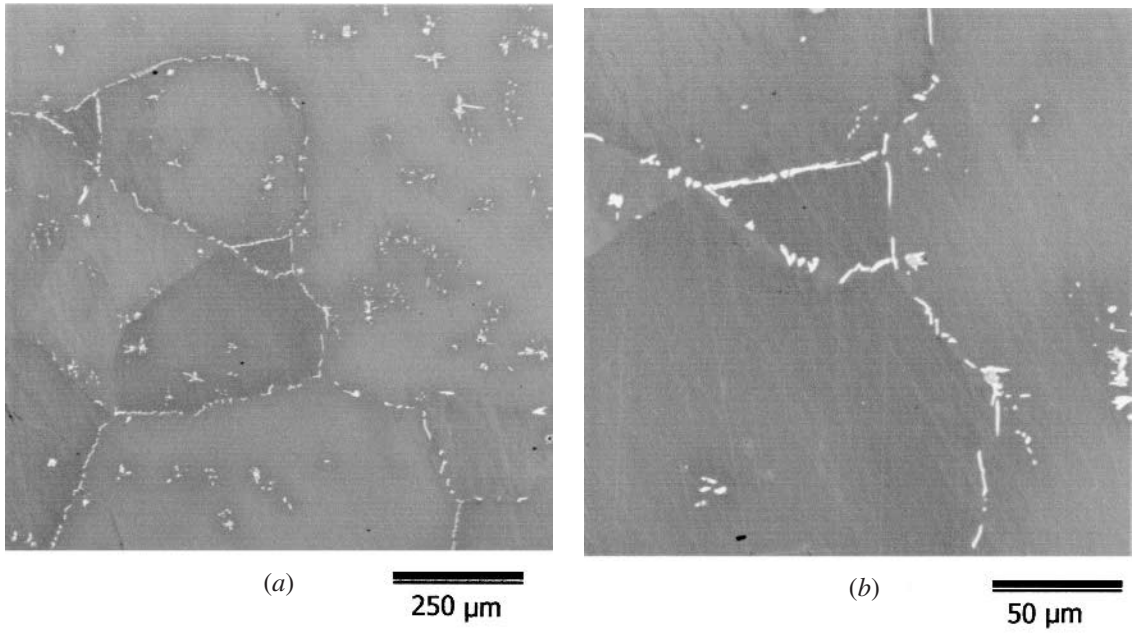

Fig. 1—(*a*) and (*b*) Microstructure of 52.5Ni-22.5Fe-25W, indicating that the composition slightly exceeds the solubility limit of tungsten in the 70Ni-30Fe base composition. Error bars represent ±1 standard deviation.

Table I. Analyzed Compositions of the Matrix (7:3 Ni-Fe) and Precipitate (W-Rich) Phases Following 24-Hour Heat Treatment at Temperatures between 800 °C and 1400 °C Followed by Ice-Water Quench

Nominal Composition (Wt Pct)	Heat Treatment	Matrix Analysis*				Precipitate Analysis*			
		Ni Wt Pct	Fe Wt Pct	W Wt Pct	Sample Size	Ni Wt Pct	Fe Wt Pct	W Wt Pct	Sample Size
49Ni-21Fe-30W	as-cast	53.7 ± 1.7	22.5 ± 0.6	21.1 ± 2.2	190	0.75 ± 0.18	0.87 ± 0.16	99.4 ± 0.9	35
49Ni-21Fe-30W	800 °C/24 h/WC	42.6 ± 0.3	28.4 ± 0.3	20.9 ± 0.4	189	0.45 ± 0.25	0.74 ± 0.13	99.1 ± 0.9	28
49Ni-21Fe-30W	1000 °C/24 h/WC	55.0 ± 0.4	21.5 ± 0.3	23.5 ± 0.4	85	2.5 ± 0.2	1.7 ± 0.2	95.8 ± 1.2	14
49Ni-21Fe-30W	1200 °C/24 h/WC	54.5 ± 0.3	23.0 ± 0.2	22.5 ± 0.4	101	4.4 ± 1.0	2.2 ± 0.3	93.3 ± 1.4	22
52Ni-23Fe-25W	1200 °C/24 h/WC	54.9 ± 0.5	22.5 ± 0.4	22.4 ± 0.6	77	2.7 ± 0.5	1.9 ± 0.4	95.9 ± 1.2	27
49Ni-21Fe-30W	1400 °C/24 h/WC	52.3 ± 0.4	21.8 ± 0.2	22.4 ± 0.5	99	1.9 ± 0.8	1.4 ± 0.1	97.2 ± 0.8	14

*Mean values ±1 standard deviation.

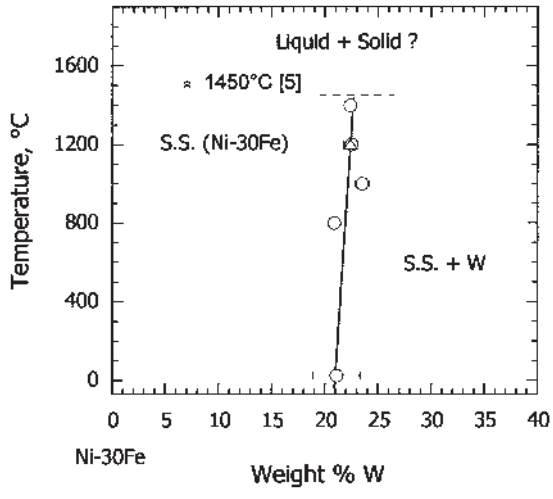

Fig. 2—Approximate solubility of W in 7:3 Ni-Fe solid solution, as determined by electron microprobe analysis of the two-phase microstructure. Standard deviations for the analyzed compositional data are indicated. The melting temperature as reported by Spencer and Mullendore[5] is indicated.

(not theoretical) calculation for each analyzed composition. With the absence of the tungsten precipitates to decorate the boundaries of the otherwise single-phase Ni-Fe matrix, the microstructure appears homogeneous and featureless in terms of contrast when BSEM and optical metallography are employed.

C. *Mechanical Behavior*

1. *Tensile behavior*

Typical stress-strain traces for the Ni-Fe-W alloys examined in this study are shown in Figure 3. In general, the alloys are characterized by moderate yield strengths (approximately 125 to 240 MPa), a high degree of work hardening leading to relatively higher values for tensile strength (approximately 320 to 485 MPa), and high ductility values (approximately 40 to 58 pct). Typically, the alloys exhibited fully ductile fracture, with final failure occurring at stresses close to zero following >85 pct reduction in cross-sectional area (pct RA). Though not resolvable in the traces provided in Figure 3, all alloys consistently exhibited serrated flow behavior (±≈2 MPa)

Table II. Analyzed Compositions of the Ingots Produced Corresponding to Nominal Percentages of 0, 30, 70, and 100 Pct of the Determined Full Solubility of W in 7:3 Ni-Fe Solid Solution

Alloy/Ingot Pct of Full Solubility	Nominal Composition (Wt Pct)	Analyzed Composition (Wt Pct)					
		Ni	Fe	W	C	O	N
0	70Ni-30Fe-0W	69.4	30.4	0.08	0.008	0.0363	0.0023
30	65Ni-28Fe-7W	65.9	28.6	5.4	0.006	0.0278	0.0010
70	59Ni-25Fe-16W	59.1	25.4	15.3	0.010	0.0200	0.0013
100	54Ni-23Fe-23W	54.1	23.1	22.6	0.020	0.0235	0.0031

Table III. Measured and Rule-of-Mixtures Density for Ingots Corresponding to Nominal Percentages of 0, 30, 70, and 100 Pct of the Determined Full Solubility of W in 7:3 Ni-Fe Solid Solution; ROM Density Was Calculated for Compositions Corresponding to Analyzed Values

Alloy/Ingot Nominal Percent of Full Solubility	Analyzed Composition (Wt Pct)	ROM Density (g/cm^3)	Archimedes Density (g/cm^3)
0	69.4Ni-30.4Fe-0.08W	8.559	8.43 ± 0.04
30	65.9Ni-28.6Fe-5.4W	8.823	8.68 ± 0.15
70	59.1Ni-25.4Fe-15.3W	9.357	9.26 ± 0.06
100	54.1Ni-23.1Fe-22.6W	9.793	9.67 ± 0.10

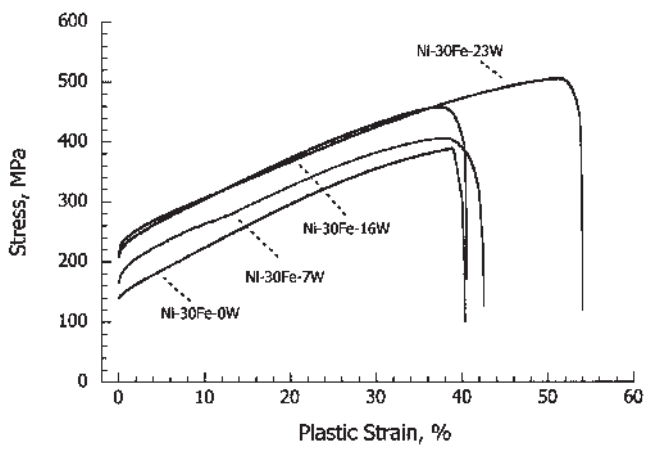

Fig. 3—Averaged stress *vs* strain traces for the alloys included in this study. These data were obtained from a conventional constant extension-rate uniaxial tension test conducted at an initial strain rate of 2×10^{-4} s^{-1}.

during plastic deformation. In some instances, upper/lower yield behavior was observed.

Figure 3 shows how the tensile data varies with composition, notably with the percentage of tungsten in solid solution. In general, higher values of tensile strength and ductility occur for alloys with higher concentrations of tungsten in solid solution. It is noted that the yield stress obtained for the fully alloyed variant (≈202 MPa) compares favorably to the value (≈195 MPa) obtained by Ekbom *et al.*[6,7] for an essentially identical composition in its as-processed form. Values for yield stress, tensile stress, and ductility as a function of the percentage of tungsten in Ni-Fe solid solution are summarized in Figure 4.

Table IV summarizes the work-hardening exponents, *n*, obtained from a fit of the tensile stress-strain data to Eq. [1]. As one might expect, the work-hardening exponent values

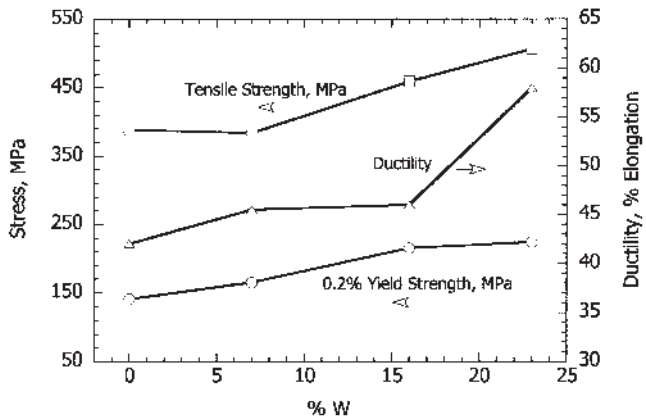

Fig. 4—Yield stress (0.2 pct offset), tensile strength, and ductility (pct elongation) as a function of percentage tungsten in Ni-Fe solid solution.

for the predominantly fcc-Ni-Fe-W solid solution alloys given in Table IV are considerably larger in their magnitude than those reported by Rabin *et al.*[2] for composite variants containing at least 88 pct of the bcc-tungsten reinforcing phase. While work-hardening behavior is larger in magnitude for monolithic matrix variants, Ekbom[7] has shown that the presence of the large tungsten particles within the WHA leads to enhanced hardening response within the matrix portion, as indicated by comparisons of hardness[7] and dislocation density[6] measurements obtained from monolithic and tungsten particle-containing variants.

2. *Strain-rate change tests*

Figure 5 illustrates a portion of a typical stress-strain trace incorporating instantaneous strain-rate changes or strain-rate jumps. As shown, flow stress tends to increase as strain rates are increased, and decrease with reductions in strain rate. Figure 5 additionally shows that the flow stress sensitivity is essentially independent of the accumulated strain in the sample, as can be shown by an extrapolation of the flow stress between common strain rates. Values for the strain-rate-sensitivity exponent, *m*, averaged over several jumps, are provided in Table IV. These data show that the strain-rate sensitivity of flow stress remains relatively constant as tungsten concentration within the Ni:Fe matrix is varied.

3. *Hardness*

The Vickers hardness for each alloy is illustrated in Figure 6.

4. *Strain aging*

A typical stress-strain trace (partial) illustrating the observed strain aging effect in these alloys is shown in

Table IV. Measured Values of the Work-Hardening Exponent, *n*, as Obtained from a Fit of the Stress-Strain Data to Equation [1] and the Strain-Rate-Sensitivity Exponent, *m*, Obtained from a Fit of the Stress–Strain-Rate Data to Equation [2]

Alloy/Ingot Nominal Percent of Full Solubility	Analyzed Composition Wt Pct	As-Cast		1200 °C/FC		1200 °C/WC		800 °C/FC		800 °C/WC	
		n	*m*	*n*	*m*	*n*	*m*	*n*	*m*	*n*	*m*
0	69.4Ni-30.4Fe-0.08W	1.081	0.012	1.246	0.010	1.048	0.010	0.892	—	1.040	—
30	65.9Ni-28.6Fe-5.4W	1.176	—	1.086	—	0.870	0.013	0.976	0.012	1.055	0.013
70	59.1Ni-25.4Fe-15.3W	1.119	0.010	1.088	—	0.851	—	1.157	—	1.004	—
100	54.1Ni-23.1Fe-22.6W	1.042	0.009	1.160	—	1.049	—	0.887	0.010	0.828	0.013

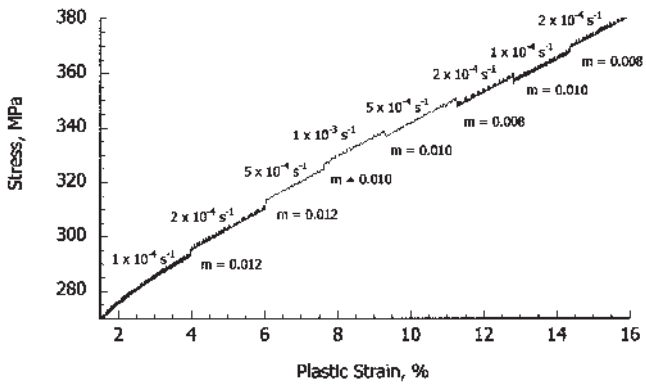

Fig. 5—Typical stress-strain trace (partial) illustrating the flow stress sensitivity on strain rate. As shown, a series of instantaneous strain-rate changes cause concomitant increases in flow stress. The resulting change in flow stress with a given change in strain rate is used to calculate the strain-rate-sensitivity, *m*.

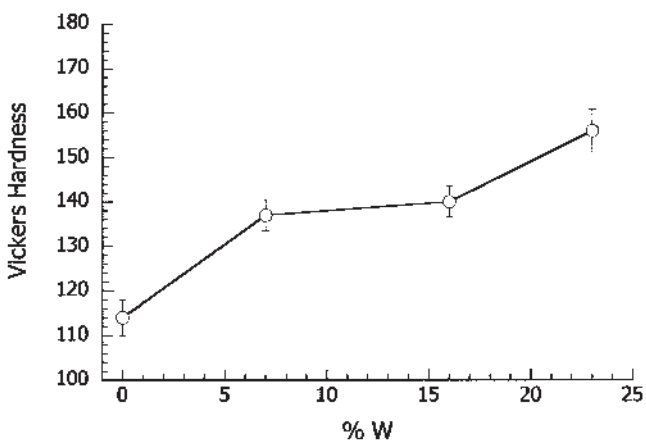

Fig. 6—Vickers hardness (50-kg_f load) as a function of percentage tungsten in solid solution. Error bars represent ±1 standard deviations.

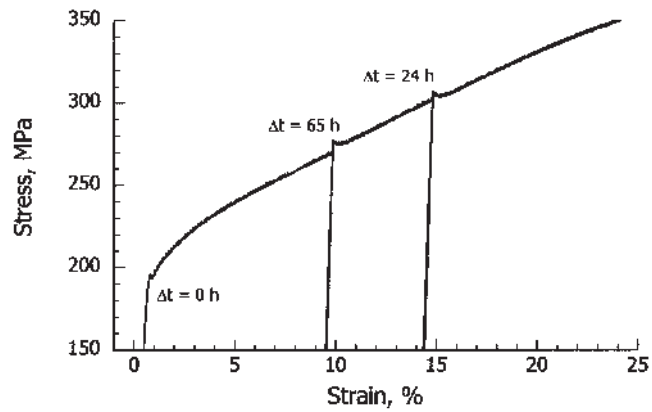

Fig. 7—The stress-strain trace (partial) illustrating the increments of strengthening that result from the indicated interruptions during the course of a tensile test. The data shown were obtained from the Ni-25Fe-16W alloy.

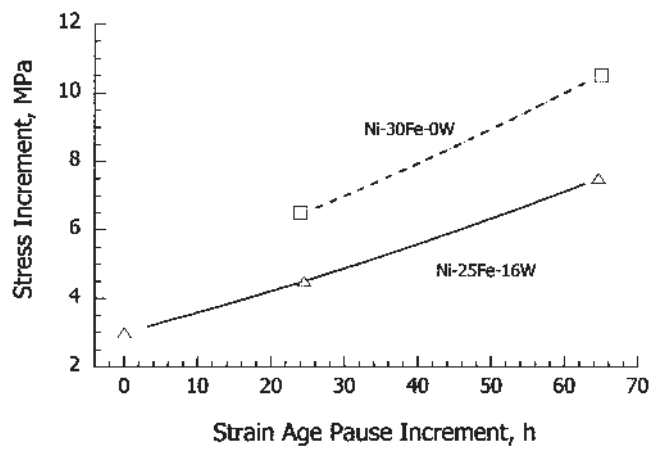

Fig. 8—The magnitude of the yielding stress increment that results following a pause in the tensile loading of the indicated alloys.

Figure 7. In Figure 7, a 65- and a 24-hour pause were imposed at approximately 10 and 15 pct strain, respectively. The magnitude of the strengthening attributable to strain aging for each of the two test samples subjected to the testing pauses is illustrated in Figure 8, which shows the stress increment as a function of the duration of the test pause. The results indicate that higher yielding increments are associated with longer pauses, but not with higher values of imposed strain (the 24-hour pauses were imposed at the larger value of strain). These results also show that the Ni-30Fe-0W alloy exhibited slightly higher yielding increments than the Ni-25Fe-16W alloy.

IV. DISCUSSION

A. *Solubility Determination*

Perhaps surprisingly, solubility was found to be approximately constant over the range of temperatures examined, *i.e.*, from 800 °C through 1400 °C. The data obtained by the

heat treatment at 1400 °C intersects the experimental conditions reported in the literature by Spencer and Mullendore,[5] who investigated the role of matrix composition (*i.e.*, Ni:Fe ratio) on melting temperature, and on the 1400 °C solubility of tungsten. These researchers report a tungsten solubility of approximately 23.5 pct at 1400 °C, essentially identical (within reasonable statistical bounds) to the 23 wt pct value determined in the present work. Ekbom *et al.*[6,7] and Woodward *et al.*[11] similarly report W solubilities in the 23 to 24 wt pct range. Based on changes in the measured lattice parameter of the matrix phase, Minakova *et al.*[14] suggests that solubility may be variable with temperature, changing from an estimated value of 25 wt pct at 1400 °C to approximately 20 wt pct following slow cooling to room temperature. The Spencer and Mullendore work also provided consistency with the observed melting temperature for the alloys in this study—notably, that 1500 °C was sufficient to melt the 7:3 Ni:Fe composition. The Spencer and Mullendore work indicates a melting temperature of approximately 1450 °C for a 7:3 Ni:Fe matrix solid solution alloy of composition 52.5Ni-22.5Fe-25W. Further, and more specifically, Bose[9] states that the eutectic temperature is approximately 1435 °C for alloys with compositions corresponding to Ni:Fe ratios of 7:3 or 8:3 Ni:Fe.

While the agreement with the work of Spencer and Mullendore[5] supports the validity of the experimental method of the present work, it is nonetheless conceivable that the true high-temperature solubility has been concealed by favorable nucleation kinetics of bcc-tungsten precipitates in the fcc Ni-Fe matrix. That is, it is possible that some of the W in solid solution at elevated temperatures has precipitated out in the form of a W-rich precipitate. In the present work, two distinct populations of W-rich precipitate were observed—a lamellar-like form populating the interior of the grains, and an apparently size- and shape-coarsened variant within intergranular regions. Lamellar precipitation usually occurs in response to the presence of a favorable (low energy) orientation relationship; this indeed appears to be active with respect to the interior precipitates since there is a preferred and aligned orientation of the precipitates within each grain. However, it is probable that the precipitates that have been retained within the intergranular regions were present at the heat-treatment temperature and exhibited time-dependent coarsening at the time of quench. It is therefore speculated that compositions within these regions likely reflect near-equilibrium conditions at the heat-treatment temperature.

B. *Mechanical Behavior*

The mechanical data presented in Figures 3 and 4 show reasonable and logical trends, in that increasing tungsten solute in solution leads to increases in yield strength, tensile strength, and ductility. In the latter instance (ductility), the solute likely serves as a soft obstacle to dislocation motion and hence serves to homogenize slip within the alloy. This is supported by the invariance to solute concentration of the work-hardening exponent, n, given in Table IV. That is, one might expect high work-hardening exponents with increasing concentration were the solute to operate more as hard obstacles.

The tensile behavior of these alloys exhibited a distinct strain-rate sensitivity of flow stress. The presence of serrated flow behavior or upper/lower yielding can often be considered indicative of an inherent strain-rate sensitivity. Similarly, the ability to exhibit a strain aging response is often, but not always, indicated by these phenomena as well. Each of these effects shares a mechanistic basis associated with interactions between solute and dislocations. Upper and lower yielding is associated with the onset of mobile dislocation activity in alloys where solute has positioned itself in dislocation cores. Strain aging is essentially identical in its mechanistic origin except that diffusion of the solute species must generally occur at rates sufficient to similarly position itself in core positions within some reasonable increment of time. Serrated yielding likewise involves solute positioning in dislocation cores, but reflects a more dynamic scenario of breakaway/attachment/breakaway/*etc*. of solute and dislocations.

Strong interactions among solute and dislocations are most frequently associated with body-centered cubic (bcc) materials, most notably, in low-carbon steels. In these materials, the effect is attributed to the presence of nitrogen solute (and carbon, but to a lesser extent). In the present study, such interactions are obviously present within the fcc Ni-rich matrix solid solution. While this may be initially surprising, a review of the literature documents strain aging in austenitic (fcc) Fe-31Ni-0.1C alloys.[15,16] In this instance, the behavior has been associated with the presence of certain critical concentrations of interstitial carbon.

Interestingly, Dowding and Tauer[17] present a summary of strengthening behavior in a series of heat-treated Ni-3Fe-90W and Ni-2.1Fe-93W alloys, and attribute measured hardness increases to strain aging that occurs *within* the *bcc*-tungsten particles during postdeformation, elevated-temperature heat treatments. Dowding and Tauer cite several other investigations, which similarly attributed an observed strain aging effect in tungsten heavy alloys to the tungsten portion, but did not specifically mention that strain aging was also possible within the matrix phase as well. These authors do not show any time dependence on the magnitude of strengthening (as noted in this study), but do reference the work of Yodogawa,[18] who shows a positive prestrain dependence of tensile strength. In the present work, it is suggested that the longer pause times enable more diffusion of the active solute species to occur. The indifference to the level of strain may indicate that the two strains were not sufficiently different as to provide a discernable effect or that there were an insufficient number of tests to properly evaluate.

Zhou *et al.*[19] also studied the behavior of a representative Ni-Fe-W matrix phase, and observed a weak strain-rate sensitivity, substantial thermal softening, and strong strain-hardening response.

The determination of the strain-rate-sensitivity exponent, m, *via* strain-rate change tests provides a means to quantify the dependence of the flow stress on strain rate. Significantly, the results exemplified by Figure 8 indicate that the flow stress increment associated with a particular rate increase remains essentially constant over a broad range of accumulated strain and stress level. Indeed, while it was stated that the value of m was essentially constant over the range of rates and strains studied, in fact, it is the stress increment that remains constant. That the increment remains constant accounts for the gradual trend of slightly decreasing m with strain (a consequence of logarithm arithmetic in the calculation of m). From a practical point-of-view, however, this

behavior enables one to obtain reasonable estimates of yield strengths at any imposed strain rate through use of a simple linear-additivity rule applied to any baseline value of yield stress.

V. SUMMARY

The solubility of tungsten within a baseline 7:3 Ni-Fe alloy was determined over a range of temperatures between 800 °C and 1400 °C. The results indicate that tungsten solubility is relatively constant over this range, and is approximately 23 wt pct.

A series of Ni-Fe-W alloys were produced with varying amounts of tungsten in 7:3 Ni-Fe solid solution. Tensile tests were conducted to determine yield stress, tensile strength, ductility, work-hardening characteristics, and strain-rate sensitivity. Hardness measurements were also conducted. Relatively consistent trends were obtained to indicate that increasing strengths and ductility are associated with higher levels of tungsten in solid solution.

The alloys featured a relatively robust strain-rate response, as manifested by a variety of observations. Serrated plastic flow behavior, upper/lower yielding, a finite value of the strain-rate-sensitivity exponent (m), and time-dependent strain aging are mutually consistent with active solute/dislocation activity in these materials.

ACKNOWLEDGMENTS

The authors offer their appreciation to Aerojet Ordnance Tennessee for providing the financial support for this undergraduate research project. The laboratory assistance of Mr. Jeffrey Haeberle is gratefully acknowledged.

REFERENCES

1. B.H. Rabin, A. Bose, and R.M. German: *Int. J. Powder Metall*., 1989, vol. 25 (1), pp. 21-27.
2. B.H. Rabin and R.M. German: *Metall. Trans. A*, 1988, vol. 19A, pp. 1523-32.
3. S.G. Caldwell: *Tungsten and Tungsten Alloys—1992*, A. Bose and R.J. Dowding, eds., MPIF, Princeton, NJ, 1992, pp. 89-96.
4. Y.H. Chiou, Y.S. Zu, and S.T. Lin: *J. Mater. Sci.*, 1996, vol. 31, pp. 4039-46.
5. J.R. Spencer and J.A. Mullendore: *Tungsten and Tungsten Alloys—1992*, A. Bose and R.J. Dowding, eds., MPIF, Princeton, NJ, 1992, pp. 111-18.
6. L.B. Ekbom, U. Lindegran, and J.-E. Andersson: *Int. J. Refractory Hard Met*., 1988, vol. 7 (4), pp. 210-14.
7. L. Ekbom: *Scand. J. Metall*., 1988, vol. 17, pp. 84-89.
8. R.S. Coates and K.T. Ramesh: *Mater. Sci. Eng*., 1991, vol. A145, pp. 159-66.
9. A. Bose: in *Tungsten and Refractory Metals—1994*, Proc. 2nd Int. Conf. on Tungsten and Refractory Metals, McLean, VA, Oct. 17–19, 1994, MPIF/APMI, Princeton, NJ, 1994, pp. 21-33.
10. R. Gero, L. Borukhin, and I. Pikus: *Mater. Sci. Eng*., 2001, vol. A302, pp. 162-67.
11. R.L. Woodward, I.G. McDonald, and A. Gunner: *J. Mater. Sci. Lett.*, 1986, vol. 5, pp. 413-14.
12. G.E. Dieter: *Mechanical Metallurgy*, 3rd ed., McGraw-Hill, Boston, MA, 1986, p. 288.
13. ASTM E92-82, "Standard Test Method for Vickers Hardness of Metallic Materials," *Annual Book of ASTM Standards*, ASTM, Philadelphia, PA, 1982, vol. 03.01, pp. 208-16.
14. R.V. Minakova, N.A. Strochak, P.A. Verkhovodov, L.G. Bazhenova, and V.L. Poltoratskaya: *Sov. Powder Met. Metal Ceram*., 1980, vol. 19, pp. 842-46.
15. M.A. Meyers and J.R.C. Guimaraes: *Metalurgia-ABM*, 1978, vol. 34, p. 707.
16. M.A. Meyers and K.K. Chawla: *Mechanical Metallurgy Principles and Applications*, Prentice-Hall, Englewood Cliffs, NJ, 1984, p. 398.
17. R.J. Dowding and K.J. Tauer: *Scripta Metall. Mater*., 1991, vol. 25 (1), pp. 121-25.
18. M. Yodogawa: *Sintering Theory and Practice*, Elsevier, New York, NY, 1982, vol. 14, p. 519.
19. M. Zhou, A. Needleman, and R.J. Clifton: *J. Mech. Phys. Solids*, vol. 42, 1994, pp. 423-58.